THE ASTROPHYSICAL JOURNAL, 556:47–58, 2001 July 20
© 2001. The American Astronomical Society. All rights reserved. Printed in U.S.A.

THE ULTRALUMINOUS M81 X-9 SOURCE: 20 YEARS' VARIABILITY AND SPECTRAL STATES

V. LA PAROLA AND G. PERES
Dipartimento di Scienze Fisiche ed Astronomiche, Sezione di Astronomia, Piazza del Parlamento 1, 90134 Palermo, Italy;
laparola@astropa.unipa.it, peres@astropa.unipa.it

G. FABBIANO AND D. W. KIM
Harvard Smithsonian Center for Astrophysics, 60 Garden Street, 02138 Cambridge, MA;
pepi@head-cfa.harvard.edu; kim@head-cfa.harvard.edu

AND

F. BOCCHINO[1]
Osservatorio Astronomico "G.S. Vaiana," Piazza del Parlamento 1, 90134 Palermo, Italy
Received 2001 February 16; accepted 2001 March 22

ABSTRACT

The source X-9 was discovered with the *Einstein Observatory* in the field of M81 and is located in the dwarf galaxy Holmberg IX. X-9 has a 0.2–4.0 keV luminosity in excess of the Eddington limit for a 1 $M_\odot$ compact accreting object, if it is at the same distance as Holmberg IX (3.4 Mpc). Past hypotheses on the nature of this super-Eddington source included a supernova remnant or supershell, an accreting compact object, and a background QSO. To shed light on the nature of this source, we have analyzed archival data, including the *Einstein* data, 23 *ROSAT* observations, and *BeppoSAX* and *ASCA* pointings. Our analysis reveals that most of the emission of X-9 arises from a pointlike highly variable source (0.5–2.4 keV $L_X \sim 2$–8×10^{39} ergs s^{-1}) and that lower luminosity extended emission may be associated with it. The spectrum of this source changes between low- and high-intensity states, in a way reminiscent of the spectra of galactic black hole candidates. Our result strongly suggest that X-9 is not a background QSO, but a bona fide "super-Eddington" source in Ho IX, a dwarf companion of M81.

Subject heading: accretion, accretion disks — black hole physics — X-rays: individual (M81 X-9) — X-rays: stars

1. INTRODUCTION

M81 is a nearby early type spiral galaxy well studied in all bands, from radio (e.g.,Beck, Klein, & Krause 1985; Bietenholz et al. 1996) to optical and UV (e.g., Ho, Filippenko, & Sargent 1996), to X-rays, where it has been observed with all the major satellites. *Einstein* observations (Fabbiano 1988) showed the presence of 10 individual X-ray sources in M81 and three sources that appear outside the optical contour of the galaxy. Among the latter ones, X-9 is the brightest X-ray source within 20′ from the nucleus of M81, with roughly half the flux of the nucleus itself. If it is at the same distance of M81 (3.6 Mpc; Freedman et al. 1994), the *Einstein* luminosity of X-9 is $\sim 3 \times 10^{39}$ ergs s^{-1}, well above the Eddington luminosity for 1 $M_\odot$ accretor in a binary system ($\sim 1.3 \times 10^{38}$ ergs s^{-1}). X-9 appears on many *ROSAT* observations of the M81/M82 region and is clearly visible in the *ASCA*-GIS field of an M81-centered observation (Ishisaki et al. 1996).

X-9 is optically coincident with the H II region MH9/10 (Miller & Hodge 1994) of the Ho IX dwarf galaxy (Georgiev 1991; Hill et al. 1993, $D = 3.4$ Mpc,), a member of the M81 group. Miller (1995) points out that the pointlike blue object reported by Fabbiano (1988) within 10″ from the X-ray source is indeed MH9/10 and reports an additional faint blue continuum object in the vicinities that he identifies as an OB association. A shock-heated superbubble with a 250 pc diameter was also found in this general area by Miller (1995), who suggested a tentative physical association between X-9 and this extended object. If X-9 is instead a compact X-ray source, its super-Eddington X-ray luminosity rules out spherical accretion onto a white dwarf or neutron star, leaving a black-hole binary as a possible candidate (e.g., Fabbiano 1995). Another possibility, advanced by Ishisaki et al. (1996) and recently explored by Ezoe et al. (2000), is that X-9 is a background quasar. Figure 1 shows the position of X-9 with respect to M81 and Holmberg IX.

In this paper we present a comprehensive study of the X-ray behavior of M81 X-9, using all the available X-ray data, with a coverage extending from 1979 to 1999. Our analysis suggests that while a faint extended source may be indeed present, most of the X-ray emission originates from a highly variable pointlike source with the spectral variability signature of a black hole binary.

In § 2 of this paper we present the data and their first reduction; in § 3 we report the results of the data analysis, including spatial structure, variability, and spectral analysis. In §§ 4 and 5 we discuss our results and draw our conclusions.

2. OBSERVATIONS AND DATA REDUCTION

Table 1 summarizes the log of all the X-ray observations of X-9. X-9 was observed with both *Einstein* HRI and IPC (Giacconi et al. 1979) in 1979 (Fabbiano 1988). It was then observed 23 times with *ROSAT* in a period of seven years from 1991 to 1998: 12 times with the PSPC (Position Sensitive Proportional Counter; Pfeffermann et al. 1987) and 11 times with the HRI (High-Resolution Imager; David et al. 1996). It was also observed in 1998 with *BeppoSAX* (Boella et al. 1997) and in 1999 with *ASCA* (Tanaka, Inoue, & Holt 1994). We therefore have observations spanning 20 yr, with good coverage in the second half of this period. With this data, we can: (1) study the temporal behavior of X-9 (using

[1] Presently at Astrophysics Division, ESA/ESTEC, Noordwijk, Netherlands; fbocchin@estsa2.estec.esa.nl

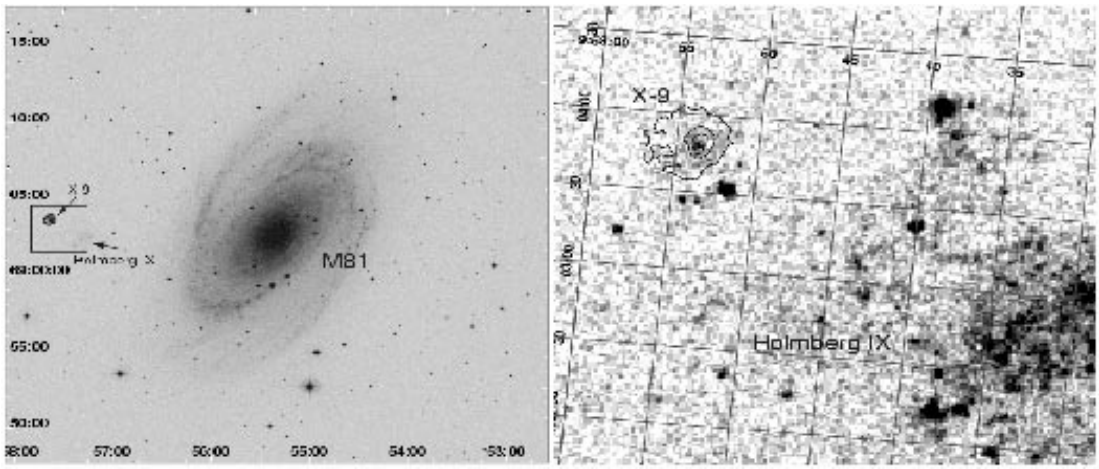

FIG. 1.—*Left:* Contour plots of HRI count rates (smoothed with a Gaussian filter with 2 pixel radius), superimposed to the optical image of M81 field. X-9 is marked by an arrow. *Right:* Enlargement of the region within the box in the upper panel shows both the position of X-9 with respect to Holmberg IX and the faint optical source coincident with the X-ray emission centroid.

all instruments for light curves and fluxes); (2) study its spectral characteristics and how they vary with time, using *ROSAT* PSPC data, as well as the wider-band, higher-resolution *BeppoSAX* and *ASCA* spectra; (3) reexamine the spatial properties suggested by Miller (1995), using the good-resolution ($\sim 7''$) *ROSAT* HRI data.

2.1. *Einstein Data*

The *Einstein* satellite observed M81 and the surrounding region in 1979. Three pointings were made: one with the IPC (Imaging Proportional Counter) in April and two with the HRI (High-Resolution Imager) in May and September.

The IPC data cover a spectral energy range spanning from 0.2 to 3.5 keV and have a spatial resolution of $\sim 1'$. The source counts were extracted from a circular region of $180''$ centered on the centroid position (Fabbiano 1988) yielding a count rate of 0.066 ± 0.003 count s^{-1}. A low-resolution spectrum can be in principle obtained from IPC data, but the source falls in a region of the detector where the spectral calibration is highly uncertain. For this reason

TABLE 1

LOG OF *Einstein*, *ROSAT*, *SAX*, *ASCA* OBSERVATION OF X-9.

Instrument	Reference	Sequence Number	Live Time	Start Date	Angle[a]
Einstein	E-IPC	2102	6515	1979 Apr 27	11.7
	E-HRI	585	19627	1979 Sep 27	12.3
ROSAT PSPC.....	1P	rp600101a00	9296	1991 Mar 25	12.7
	2P	rp600110a00	12717	1991 Mar 27	38.6
	3P	rp600052n00	6588	1991 Apr 18	31.1
	4P	rp600110a01	12238	1991 Oct 15	38.6
	5P	rp600101a01	11085	1991 Oct 16	12.7
	6P	rp600382n00	27120	1992 Sep 29	12.7
	7P	rp180015n00	17938	1993 Apr 03	13.5
	8P	rp180015a01	8731	1993 May 04	12.5
	9P	wp600576n00	16412	1993 Sep 29	19.5
	10P	rp180035n00	17800	1993 Nov 01	12.5
	11P	rp180035a01	4234	1993 Nov 07	12.5
	12P	rp180050n00	1849	1994 Mar 31	12.5
ROSAT HRI	1H	rh600247n00	26320	1992 Oct 23	12.5
	2H[b]	rh180015n00	1688	1993 Apr 16	12.5
	3H	rh600247a01	21071	1993 Apr 17	12.5
	4H	rh600739n00	19902	1994 Oct 19	12.5
	5H	rh600740n00	18984	1995 Apr 13	12.5
	6H	rh600881n00	14826	1995 Nov 12	12.5
	7H	rh600882n00	18328	1996 Apr 15	12.5
	8H	rh600882a01	5091	1996 Nov 27	12.5
	9H	rh601001n00	19231	1997 Mar 29	12.5
	10H	rh601002n00	12590	1997 Sep 30	12.5
	11H	rh601095n00	12590	1998 Mar 25	12.5
BeppoSAX	MECS	40732001	100287	1998 Jun 04	13′
	LECS		43931		
ASCA.....	SIS	57048000	33000	1999 Apr 06	5′

[a] Off-axis angle of the source on the detector.
[b] Sequence 2H was not used (see text).

we used these data only to derive an estimate of the source flux, using the spectral models suggested by the other available spectral data (see § 3.3 and Table 4 for details).

The *Einstein* HRI has a spatial resolution of $\sim 3''$ and no spectral resolution. Photons from M81 were collected during two different observing period, then merged in the same file. However, the two relevant pointings are slightly offset. For this reason X-9 is in the HRI field only in the September data. The source counts (that thus refer just to September, as well as the exposure time in Table 1) were extracted from a 18″ radius circle centered on the source centroid and the count rate is ~ 0.12 counts s^{-1}. For full details on source counts and background extraction and events corrections we refer to Fabbiano (1988).

2.2. *ROSAT Data*

ROSAT data were processed using the IRAF(v. 2.11)/PROS (v. 2.5) software system (Tody 1986; Worral et al. 1992). The twelve PSPC observations (see Table 1) were aligned using the nominal pointing directions. The result was then checked by comparing the position on the image array of three bright sources in the field of view. In order to achieve a better signal-to-noise ratio when determining the source position, the eight M81-pointed observations were co-added and the wavelet detection algorithm (Damiani et al 1997) used in the GALPIPE pipeline analysis of *ROSAT*/PSPC data (Mackie et al. 1995) was applied to the co-added image. This algorithm is based on the application of a set of wavelet transforms of the image, evaluated on different radii, and allows the detection of both pointlike and extended sources, the determination of source centroid position, and an estimation of its count rate and size. The remaining four PSPC sequences (2P, 3P, 4P, 9P) were not used in this process because they show X-9 at a large off-axis angle, so that the source image is highly degraded. The centroid coordinates were found to be $9^h57^m54^s$ R.A. and 69°03′46″ Decl. The average count rate of the source is 0.196 ± 0.002 count s^{-1}, with a total exposure time of 146 ks. The source radius (3.′25) was chosen to be the point where the radial profile of the source (in 20″ bins) become consistent with the value of the field background (extracted from the source-subtracted image, from an annulus centered on the centroid position of the nucleus of M81, with radii 540″ and 600″). The same co-added image was used to extract the spectral information (see § 3.3). In order to conduct the different steps of time analysis, we examined the source emission in each individual observation. The radius for source photon selection depends on the position of X-9 on the detector plane, because of the increase of the radius of the PSF with increasing distance from the detector center (Boese 2000). For the off-axis observations we used the source radius evaluated with the GALPIPE processing applied on each observation: 4′ to 5′ where X-9 position is between 20′ and 40′ away from the detector center. We have excluded any part of the selected region obscured by the instrumental PSPC "ribs."

The source is also visible in eleven HRI observations pointed on M81, with a total exposure time of 177 ks and an average count rate of $(5.31 \pm 0.09) \times 10^{-2}$ count s^{-1}. Among these, sequence rh180015n00 (2H in Table 1) has been excluded from the analysis because we were not able to detect any source in the whole field of view with the detection algorithm in the IRAF/PROS task *xexamine*, probably due to its short exposure time. This made it impossible to align this sequence with the other ones. The remaining observations were aligned by comparing and aligning the position of three bright sources in the field of view. The task *xexamine* was used to find the source centroid position from the longest live time observation (1H). The X-9 source coordinates are $9^h57^m54^s.3$ R.A. and 69°03′46.″4 Decl., well within the error box associated with the PSPC detection. Thus the two determinations are consistent with each other, and from now on we will use the more accurate HRI centroid coordinates. For each observation, source counts were extracted from a circular region with 1.′3 radius, as found with the *ldetect* IRAF/PROS algorithm (S. Dyson 1999, private communication).

2.3. *BeppoSAX Data*

X-9 is visible in the *BeppoSAX* observation of M81 performed on 1998 June 5 (Pellegrini et al. 2000). The observation was processed with the SAXDAS software version 1.6.1 applying the standard corrections and event selections. It includes data from the Low (LECS; Parmar et al 1997) and the Medium (MECS; Boella et al. 1997) Energy Concentrator Systems, which are sensitive in the 0.1–10 keV band (0.1–4.5 and 1.6–10.0 keV, respectively), have an angular resolution of 2′ FWHM, and an energy resolution $\Delta E/E = 0.08$ (FWHM) at 6 keV. The LECS and MECS exposure times are 23 and 69 ks, respectively.

We have extracted the LECS spectrum of X-9 from a circular extraction region with radius of 4′, which ensures that we collect at least 80% of the photons of this faint source. The extraction region is centered at $9^h57^m52^s.7$ R.A., +69°03′47″ Decl. (J2000). The background was collected from a ring with inner and outer radii of 10.′5 and 13.′8, respectively, centered on the on-axis position, excluding the X-9 source regions defined above. The spectrum was rebinned to have at least 20 counts per energy bin. We have generated the LECS response matrix and ancillary response file using the task *lemat* in the LHEASOFT Release Version 5.0.1. We have taken peculiar care in the analysis of the MECS data, because of the partial source obscuration by the support ribs. A small 2′ extraction radius was chosen to exclude the ribs, and the MECS2 and MECS3 spectra were extracted separately. We have verified that, even with this small extraction region, the MECS3 spectrum is still severely distorted by the rib obscuration and therefore we have chosen to use only the MECS2 spectrum. We have used the standard MECS response matrix and the ancillary response file for an off-axis source located at 14′ (X-9 is at $\sim 12'$ off-axis) and an extraction radius of 2′, created using the on axis 2′ extraction radius file available from the *Sax* Data Center and correcting for the energy dependent vignetting effect. MECS background selection and rebinning are similar to those of the LECS.

2.4. *ASCA Data*

ASCA observed X-9 in 1999; all instruments were active. For this analysis, we used the archival event files, with the default screening and event selection criteria. During the observation the GIS detectors (Gas Imaging Spectrometer; Kohmura et al. 1993) were in the PH normal mode. The source counts were extracted from a 6′ circular region around the source centroid, and the background was subtracted from a source-free circular region in the same field. The count rates for the two GIS detectors in the (0.5–10.0) keV band are 0.217 ± 0.003 (GIS2) and 0.270 ± 0.003

(GIS3) count s^{-1}, for an integration time of 38 ks. For the spectral analysis, the most recent publicly released response files were used for each detector. We also estimated the expected contamination from the nucleus of M81 in the extraction region of X-9, using the calibration image of Cyg X-1 provided by the HEASARC. We estimate that at least 7% of the counts extracted from the X-9 region belongs indeed to the nucleus of M81.

The two SIS (Solid State Imaging Spectrometer; Burke et al. 1991) detectors were observing in 1CCD BRIGHT mode. Chip 1 on SIS0 and chip 3 on SIS1 were active. We extracted the source counts from a 4′ circular region around the source centroid. The contamination due to photons from the nucleus of M81 (which falls outside the chip) is less than 0.02% (K. Ebisawa 2000, private communication). The background photons were collected from the source-free region of each chip in the same observation. The response matrix and ancillary file were produced with the FTOOLS *sisrmg* and *ascaarf* (FTOOLS v3.5), separately for each detector. The two SIS count rates for X-9 are 0.350 ± 0.004 (SIS0) 0.288 ± 0.003 (SIS1) count s^{-1}, for an integration time of 33 ks.

We then compared the SIS and GIS spectra in order to estimate the amount of contamination from the nucleus of M81 to the spectrum of X-9 in the GIS data. The GIS spectrum shows a well-detectable soft excess over the SIS spectrum. As the four instruments onboard *ASCA* observe the target simultaneously, this difference cannot be due to an intrinsic variation of the source emission: the most likely explanation is instead contamination from the nuclear source. In order to check this hypothesis we extracted the spectrum of the nucleus of M81 from the two GIS fields (the radius of the extraction region is 6′). This spectrum is very well described by a power law with $\Gamma = 1.80^{+0.02}_{-0.01}$ ($\chi^2/\nu = 314/326$). We used this model to fit the soft excess found in the GIS data when the overall spectrum is modeled with the best-fit SIS parameters (see § 3.3 and Table 4 for details). This excess amounts to $\sim$20% of the total photon flux, which is twice the expected contamination. As we where not able to fully explain the difference between the observations with the two instruments, we decided to exclude the GIS data set from the following analysis, retaining only the SIS data.

Incidentally, we note that in this observation (1999) the nucleus of M81 appears to be in a different spectral state with respect to that of the 1993 observations, reported by Ishisaki et al. (1996), where a thermal component was needed, in addition to the power law, to fit the observed spectrum.

3. ANALYSIS AND RESULTS

3.1. *Spatial Properties*

In order to establish the nature of X-9, it is very important to determine its shape and extension. Our wavelet detection analysis (see § 2.2) suggests a radius of 3.′25 for this source in the PSPC image, which is larger than the predicted PSF radius for the relevant off-axis angle (Boese 2000) and suggests that X-9 could have an extended component: to check this hypothesis we used the better angular resolution HRI data. The main difficulty in this analysis is that X-9 is 12.′5 off axis, therefore the analytical formula for the bidimentional point spread function cannot be used, and alternative methods must be applied. We analyzed the data from the HRI sequence 1H (which has the longest live time) and compared the results to those from the pointlike calibration source HZ43, whose data are in the IRAF calibration database. We chose the HZ43 observation at 12′ off-axis, which has the off axis angle closest to that of X-9. We did not use the co-added file obtained from the 10 available observations of X-9, in order to avoid any small misalignment that could possibly affect the co-added image. As a first step, we applied to the 1H data the aspect correction required for data processed before the SASS7-B release[2] as well as the dewobbling procedure of Harris et al. (1998). We found that this correction does not appreciably affect the data. The source centroid position, determined using the detection algorithm in the IRAF/PROS task *xexamine*, is $9^h57^m54^s.3$ R.A. and $69°03'46''.4$ Decl.

The X-ray contours of the calibration HZ43 image, smoothed with IRAF *imsmooth* with a 2 pixels Gaussian function, show that the PSF is distorted, with a larger width in the direction of the center of the detector (Fig. 2, *left*). The contours from the 1H image, smoothed in the same way, show a similar distorted shape with comparable extension, but because of the smaller S/N ratio, the shape is less well determined (Fig. 2, *right*). To compare the radial profile of the two sources, we selected two angular sectors (see Fig. 2) centered on the source centroid positions: the internal one is in the direction of the detector center and the external one in the opposite direction. The relevant angles were selected on the calibration image and then reported on the X-9 image. Counts were then extracted, for each sector, from 60 annuli each 2″ wide around the source centroid, for a total radius of 2′. In order to make a direct comparison of the two profiles, both were normalized to the total encircled counts within a 2′ radius. In Figure 3 we plot both the internal and the external profiles for the two sources. In both profiles X-9 appears more extended than HZ43. In particular between 10″ and 20″ of the external sector there is an evident excess of X-9 with respect to the calibration curve that is well below the error bars. This excess corresponds to about 10% of the total emission, i.e., a luminosity of $\sim 2.5 \times 10^{38}$ for a line of sight galactic $N_H = 4.1 \times 10^{20}$ cm^{-2}, assuming a 1 keV thermal spectrum at the distance of Holmberg IX. This has led us to the conclusion that X-9 is likely to be a composite source, including a point like component (as supported by the time variability analysis, see next section) and diffuse emission, which may be physically unrelated.

The comparison of the HRI image with the optical one from the POSS II archive confirms the coincidence of the center of the brightest X-ray contour with the faint blue object reported by Fabbiano as the probable optical counterpart of X-9 and identified by Miller (1995) with the H II region MH9/10 (Fig. 1). Henkel et al. (1996) estimated the magnitude of this object (that appears extended on a size of 20″) to be $m_B = 20^m.1 \pm 0^m.1$. However, the angular resolution of our data is still insufficient to give strong constraints on the spatial distribution of X-9 and to argue on a physical association between the X-ray emission and the optical object.

3.2. *Time Variability*

We studied the temporal evolution of X-9 using *Einstein*, *ROSAT*, *SAX*, and *ASCA* data. Source and background photons were extracted as explained in § 2. Our data cover a

[2] From http://hea-www.harvard.edu/rosat/rsdc_www/aspfix.html.

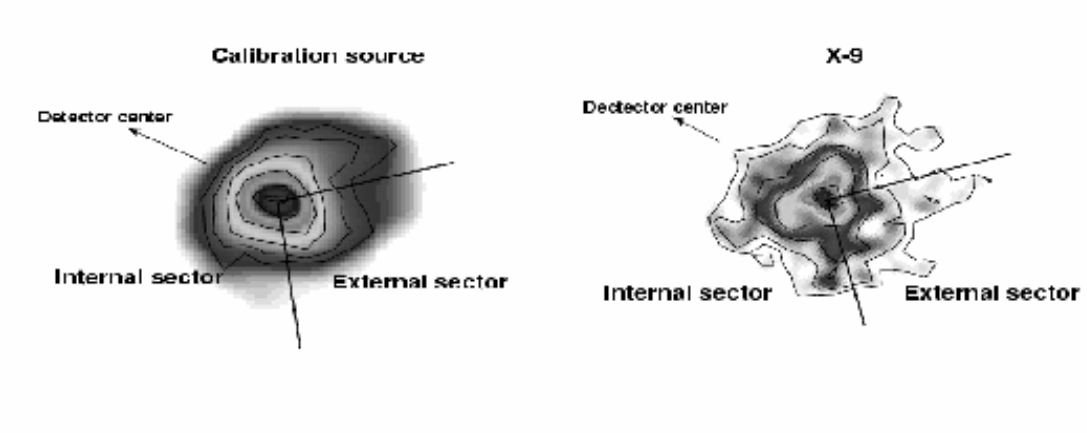

FIG. 2.—*Left:* Contour plots of HZ43 calibration source counts on *ROSAT* HRI at 12′ off axis, where the asymmetric structure of the PSF is evident. *Right:* Contour plot of X-9 counts have been rotated to have the same position as HZ43 respect to the detector center. Sectors used for the radial profile extraction are also shown, as well as the direction of the detector center.

period of 20 yr spanning 1979 April to 1999 April. We searched for short scale variability within each observation with a Kolmogorov-Smirnov and a Cramer-von Mises variability test. We excluded from this analysis the four PSPC off-axis observations, as the position of the source on the detector makes the light curve much more affected by the strong background variations caused by the detector wobbling. We report the results in Table 2. In four observations out of 22 we detected variability with, at least, 90% confidence with both tests. We performed the same tests on the background field in the vicinity of the source, finding that the background emission is variable as well, with a typical timescale of the order of 10^3 s. This timescale was estimated from the oscillations of the background counts around the curve of uniform distribution hypothesis and then compared with that of the source (evaluated in the same way). We found that in all cases there is no evident matching between the background and source timescales, and we conclude that the source variability we find is real, not an artifact due to background variability. To check further the consistency of our results, we performed a different test (Collura et al. 1987) based on χ^2 statistics applied on the background subtracted light curves (created in 200 s bins) for each observation. This test also checks for the variability timescale through a pulse model. We thus consider to be variable only those observations with more than 90% chance of variability and with at least two methods. This includes observations 6P, 7P, 10P, 3H, 11H. From the

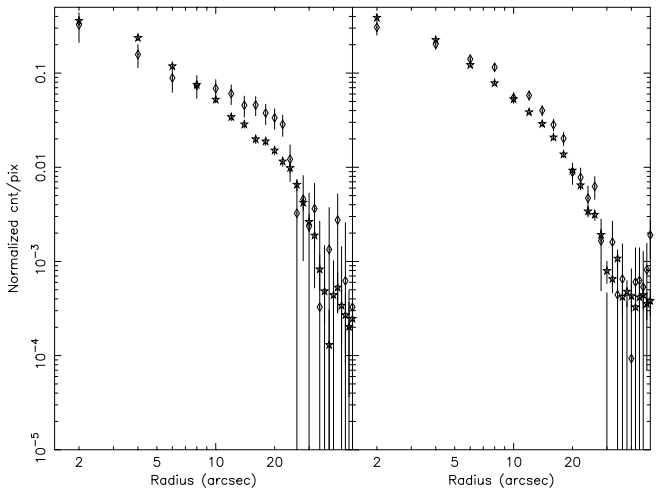

FIG. 3.—Radial profile of the calibration source HZ43 (*stars*) compared to X-9 profile (*diamonds*). *Left:* External sector. *Right:* Internal sector. Data points are normalized to the total number of counts within 2′. Extraction annuli are 2″wide (1 detector pixel = 0.″5).

TABLE 2

VARIABILITY TESTS ON INDIVIDUAL SEQUENCES

Sequence Reference	Kolmogorov-Smirnov Test	Cramer-von Mises Test	Collura	Variability
E-IPC ...	NO	NO	NO	
E-HRI ...	NO	95%	NO	
1P	NO	NO	90%	
2P	...	...	...	
3P	...	...	95%	
4P	...	...	...	
5P	NO	NO	95%	
6P	99%	95%	99%	×
7P	99%	99%	99%	×
8P	NO	NO	NO	
9P	...	...	...	
10P	NO	95%	99%	×
11P	NO	NO	NO	
12P	NO	NO	95%	
1H	NO	NO	90%	
3H	99%	95%	90%	×
4H	NO	NO	NO%	
5H	NO	NO	90%	
6H	NO	NO	NO	
7H	NO	NO	90%	
8H	NO	NO	NO	
9H	NO	NO	...	
10H	NO	NO	...	
11H	90%	90%	90%	×
SAX	NO	...	...	
SIS.....	NO	NO	...	

NOTE—For those observations found variable with more than 90% probability, the variability confidence level is quoted. NO means no variability found; ellipses mean that the test could not be applied because of strong background variability or unsufficient statistics. Variable observations are flagged with crosses ion the fourth column.

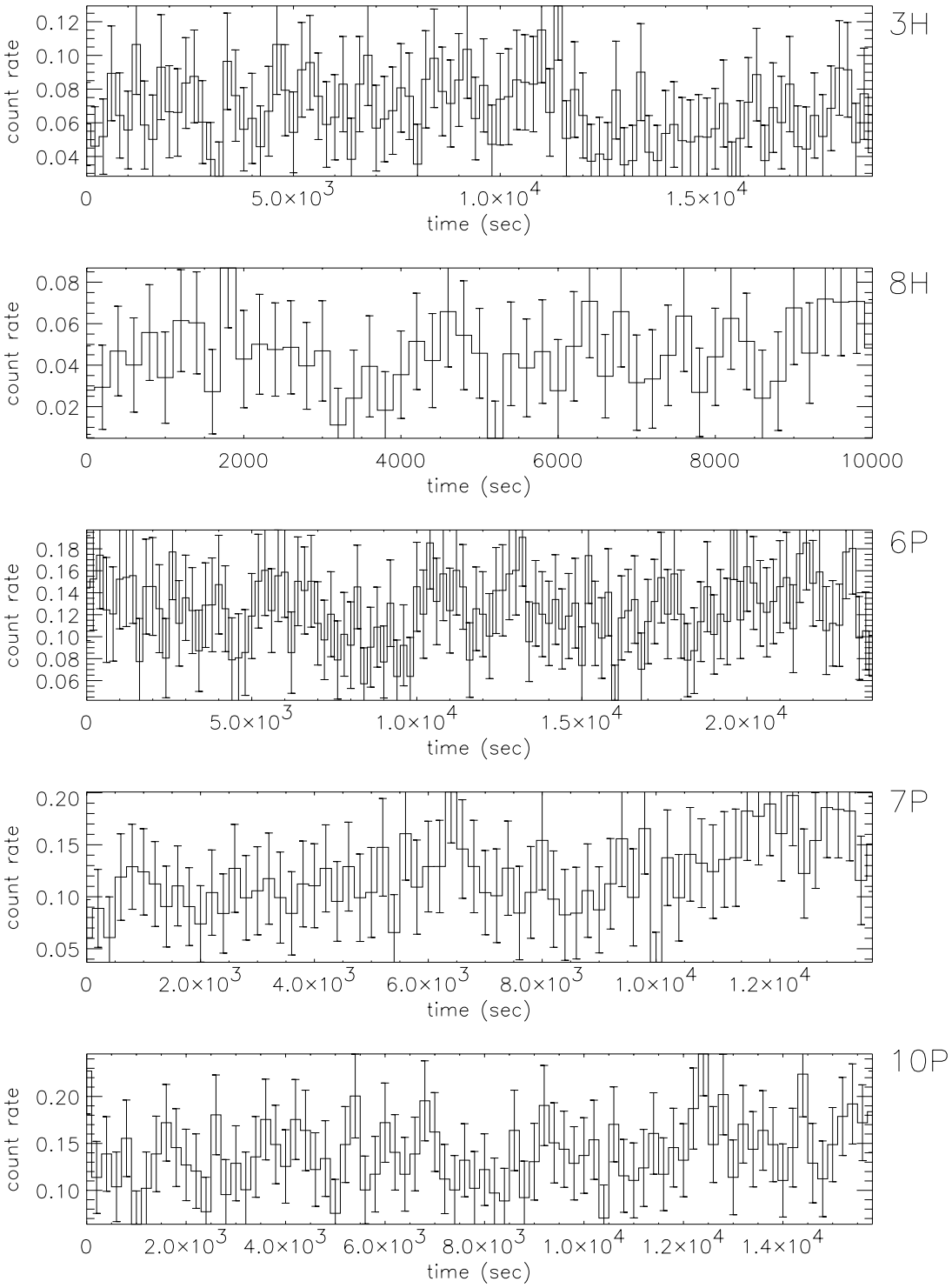

FIG. 4.—Individual light curves in 200 s bins of the variable observations (identified by the code on the right of each plot). For clarity of presentation only the GTI are plotted.

inspection of the individual light curves (Fig. 4) there is no striking evidence of either periodic or flarelike variability features. In the observation 7P we observe a steadily increasing source flux.

In order to study long-term variability, we compared data from the different instruments using all the available observations. Source counts were extracted from each observation, as described in § 2, after correcting for the appropriate exposure map. Exposure maps for *ROSAT*/HRI were created using the analysis procedure tools developed by Snowden et al. (1994). For each PSPC observation we calculated the source flux in the (0.5–2.4) keV energy band using the parameters that best fit the PSPC spectra (see § 3.3 and Table 4 for full details). For *ROSAT*/HRI and *Einstein* (IPC and HRI) observations we adopted the model used for PSPC data, correcting for the different count rate and instrumental response. The appropriate best-fit models were used for *ASCA* and *SAX*. All fluxes were calculated in

the (0.5–2.4) keV band. Results are reported in Figure 5, where each data point corresponds to one observation. Here we note that, in spite of being taken with different instruments, HRI and PSPC data are in good agreement, and this is particularly evident in the period that covers 1992 April. Moreover *SAX* data are consistent with the trend shown by the last HRI observations, while the *ASCA* point shows a much higher flux. The source flux is clearly variable: in Figure 5 there is evidence of variability on timescales of months as well as a descending trend on longer timescale (few years) broken by some flarelike episodes. The data do not show any hint of periodical variability. A flare or a change in the physical status of the source could be responsible for the two high-luminosity episodes shown by the two HRI observations 8H and 9H (at $\sim 5.05 \times 10^4$ MJD) and by the *ASCA* observation.

We also searched for spectral variability in the PSPC data, by evaluating two different hardness ratios, both defined as

$$HR = \frac{\text{hard} - \text{soft}}{\text{hard} + \text{soft}}, \quad (1)$$

using for each the energy bands showed in Table 3. We decided to use two different spectral hardness ratios because the first gives a measure of the spectral hardness over the whole PSPC band, while the second allows us to probe the spectral behavior of the high-energy part of the *ROSAT*/PSPC band. We did not use the data from *ASCA*, *BeppoSAX*, and *Einstein*, as the statistics of X-9 allows to obtain only a single point from each observation and we cannot compare points from different instruments. We plot both hardness ratios in Figure 6. We find no significant variability of the hardness ratios, with the exception of a single point (observation 4P) showing a softer spectrum in the high-energy band ratio (HR2).

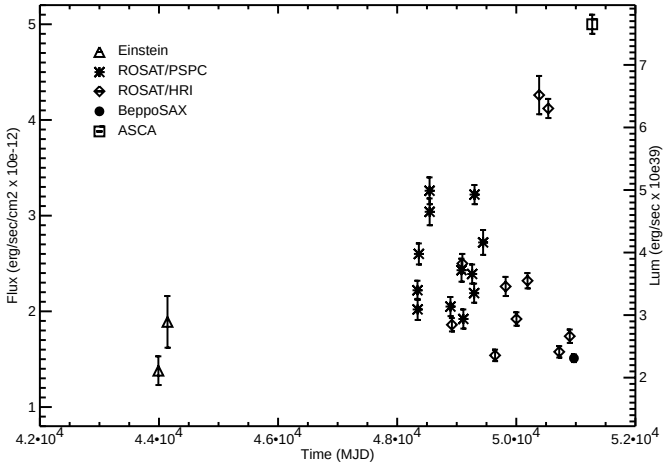

FIG. 5.—X-9 flux between 0.5 and 2.4 keV as a function of time. See text for details on flux calculation. The luminosity assumes a distance of 3.4 Mpc.

TABLE 3

DEFINITION FOR HARDNESS RATIO BANDS

Band	Soft band	Hard band
Whole band (HR1).....	0.11–0.42 KeV	0.52–2.02 KeV
Hard band (HR2)	0.52–0.91 KeV	0.91–2.02 KeV

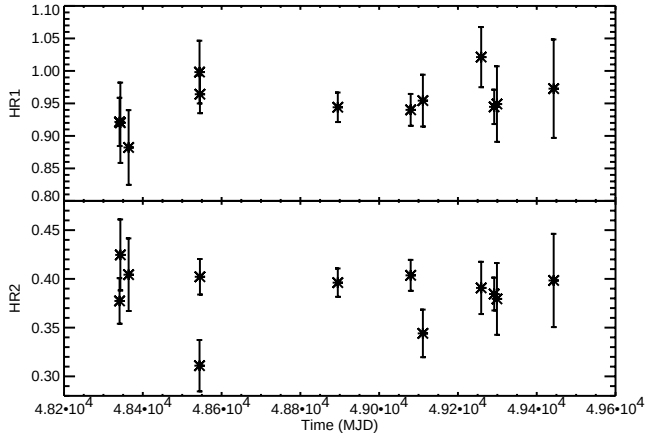

FIG. 6.—Hardness ratios HR1 and HR2 for X-9 in M81 from *ROSAT*-PSPC data. Ratios HR1 and HR2 are defined as hard−soft/hard+soft (see Table 3).

3.3. *Spectral Analysis*

We have performed model-fitting analysis of PSPC, *BeppoSAX*, and *ASCA* spectral data of X-9. In order to achieve a good S/N ratio we summed the eight *ROSAT*-PSPC pointed observations of M81. PSPC Spectra were extracted from a circular region with radius 360′; background is from an annulus centered on the source, with radii 360′ and 500′ (internal and external respectively), excluding the slice falling on the instrumental rib. Spectral data from the *BeppoSAX* and *ASCA* observations were extracted as explained in § 2. We have thus obtained different spectra over a total energy range going from 0.2 to 10.0 keV. The analysis was performed using the XSPEC v.10 software tool (Arnaud, George, & Tennant 1992).

We examined several hypotheses to explain the strong X-ray emission of X-9, including the possibility that X-9's super-Eddington luminosity is the signature of an accreting black hole (see Fabbiano 1995). We used the following spectral models to fit the spectra from the different instruments:

1. an absorbed power law (adequate to the hypothesis of a quasar or an X-ray binary);
2. a Raymond spectrum with one or two temperatures (that could describe a supershell component);
3. a multicolor black body disk (MCBB)—adequate to a black hole candidate, as in Makishima et al. (2000).
4. different combinations of the above models to check for multiple components.

The fit results are shown in Table 4. The quoted errors for the spectral parameters correspond to the 90% confidence level for 1 interesting parameter. We first analyzed separately the different data sets (*ROSAT*/PSPC, *SAX*/LECS+MECS, *ASCA*/SIS). A simple power law gives a good fit for the PSPC and an acceptable fit for the *SAX* data, but with very different photon indexes (2.24 ± 0.24 for PSPC and ~ 1.4 for *SAX*). This could be the signature of either strong spectral variability or the presence of a soft component not immediately recognizable in the *SAX* data. In particular, the best fit for the MECS data is a power law with $\Gamma = 1.40 \pm 0.20$. The same simple model can be used to acceptably fit the composite MECS+LECS spectrum, obtaining $\Gamma = 1.37 \pm 0.18$. We also checked for the presence of a Fe Kα line, by adding to the power-law model a Gaussian line with fixed energy either at $E = 6.4$ keV or

TABLE 4

SPECTRAL ANALYSIS: FIT RESULTS

Model	Instruments	$n_H(\times 10^{22})$[a]	Γ[b]	T (keV)[c]	χ^2_ν(Prob)[d]	ν[e]
1.....	MECS	$0.04^{+0.6}$	$1.40^{+0.19}_{-0.22}$	...	1.48 (0.05)	27
2.....	MECS	$0.04^{+0.6}$	1.42 ± 0.16	...	1.38 (0.10)	26
1.....	MECS+LECS	$0.08^{+0.12}_{-0.04}$	$1.37^{+0.18}_{-0.17}$	...	1.22 (0.15)	44
3.....	MECS+LECS	$0.3^{+0.5}_{-0.3}$	$1.28^{+0.28}_{-0.36}$	$0.28^{+0.40}_{-0.06}$	1.20 (0.18)	42
4.....	MECS+LECS	$0.06^{+0.10}_{-0.02}$	...	28^{+50}_{-14}	1.19 (0.18)	44
5.....	MECS+LECS	$0.04^{+0.03}$	...	$3.0^{+0.7}_{-0.5}$	1.62 (0.00)	45
1.....	PSPC	0.22 ± 0.05	2.24 ± 0.24	...	0.71 (0.88)	29
4.....	PSPC	0.085 ± 0.010	...	$4.8^{+1.2}_{-0.7}$	1.42 (0.06)	28
5.....	PSPC	$0.10^{+0.03}_{-0.02}$	...	$0.60^{+0.06}_{-0.07}$	0.89 (0.63)	29
3.....	MECS+PSPC	$0.18^{+0.13}_{-0.07}$	$1.32^{+0.22}_{-0.38}$	$0.29^{+0.16}_{-0.11}$	1.04 (0.40)	56
1.....	*ASCA* SIS	$0.48^{+0.02}_{-0.03}$	2.15 ± 0.04	...	1.53 (0.00)	318
4.....	*ASCA* SIS	$1.01^{+0.19}_{-0.04}$	$2.58^{+0.07}_{-0.08}$	$0.119^{+0.018}_{-0.008}$	1.25 (0.00)	315
5.....	*ASCA* SIS	0.177 ± 0.015	...	1.24 ± 0.03	1.13 (0.05)	318

NOTE—The first column contains the model description according to the following code: (1) power-law; (2) power-law+Gaussian line (with energy fixed at 6.4 keV) ; (3) power-law+MCBB; (4) Raymond-Smith thermal model (+power law where needed); and (5) MCBB.

[a] Column density. The lower limit is set to 4.1×10^{20} cm^{-2}, i.e., the galactic line of sight value.

[b] Power-law photon index.

[c] Temperature of the MCBB or of the Raymond spectrum, whichever of these models have been used.

[d] Reduced χ^2_ν and probability value.

[e] Number of degrees of freedom.

$E = 6.7$ keV. The F-test performed after adding the line at $E = 6.4$ keV (the best choice) indicates that adding this component is not justified if we retain 5% of F-test probability value as the confidence level for significative component addiction.

An alternative model for PSPC data is the MCBB, with a temperature of 0.60 ± 0.06 keV. This model also gives an acceptable fit for *ASCA* data, with $T = 1.24 \pm 0.03$ keV, but is not adequate to fit the *SAX* data ($\chi^2/\nu = 73/45$).

We also made the assumption that the soft spectrum does not vary in the time span from the set of PSPC observations to the *SAX* observation, since we see no significant variability in the PSPC hardness ratio and a rather small flux difference between PSPC and *SAX* measurements (see Fig. 5). With this assumption we made a simultaneous fit of PSPC and MECS data, finding that an excellent fit can be obtained with a power-law with $\Gamma = 1.32^{+0.22}_{-0.38}$ plus a disk component (i.e., an MCBB), with $T = 0.29^{+0.16}_{-0.11}$ keV. The same model was then used to fit LECS+MECS and *ASCA*/SIS data. For LECS+MECS data we find a marginal improvement (F-test probability of 4%) of the fit probability related to the reduced χ^2, with respect to the simple power-law model, and a set of fit parameters in very good agreement with those found for PSPC+MECS. For *ASCA*/SIS data the spectrum appears dramatically different: a much higher temperature for the disk component ($T = 1.24 \pm 0.03$ keV) is needed than for the other data sets, and there is no evidence for the presence of a power-law component.

The Raymond-Smith model (marked 4 in Table 4), gives a good fit only to the *SAX* data, but with a very high kT (basically confirming the hard power law), incompatible with the soft emission that may be expected from a superbubble (e.g., Wang & Helfand 1986; Wang & Chu 1999). Moreover, if we consider the results obtained with this model for the observations made with the other instruments, we find strong variations both in the temperature and in the emission measure. The latter is given as the model normalization (multiplied by a factor containing the distance), and we find that the three normalizations relevant to each instrument are not compatible with each other. The same happens for the temperature where the one found with *SAX* is at least 1 order of magnitude higher than that found with the two other data sets. As we do not expect such a high spectral variability in a few years period from a supernova remnant, we can confidently reject this model as inadequate to account coherently for all the spectra we observe.

Concluding, the most plausible scenario for the spectral behavior of X-9 is that of a composite power law+MCBB, where the MCBB temperature and emission measure increase with increasing source luminosity.

4. DISCUSSION

Although $\sim 10\%$ of the emission observed in the *ROSAT* HRI could be extended, the temporal and spectral characteristics of X-9 strongly suggest that most of the emission is due to a compact object. The strong variability (up to a factor of ~ 4 in a monthly timescale) observed in the X-9 light curve (Fig. 5) excludes the hypothesis of supernova emission and points to a compact X-ray source. From the analysis of the spectral data sets, we see that this flux variation is correlated with a spectral variation.

The spectral behavior of X-9 let us conclude that this source is not a far-away background QSO (as suggested by Ezoe et al. (2000), who analyzed a set of *ASCA*/GIS data pointed on M81), but rather an ultraluminous binary in Ho IX. The best-fit temperature from the *ASCA* spectrum ($T \sim 1.2$ keV) is well in excess of the typical values we would expect from active galactic nuclei (AGNs) ($T \lesssim 0.1$ keV for $M > 10^6\, M_\odot$; Piro, Matt, & Ricci 1997). Moreover, the *BeppoSAX* low state spectrum (Fig. 7) shows a very hard power law ($\Gamma \sim 1.3$), by far harder than the $\Gamma \sim 1.7/2.0$ power law seen in AGN spectra (Reynolds 1997).

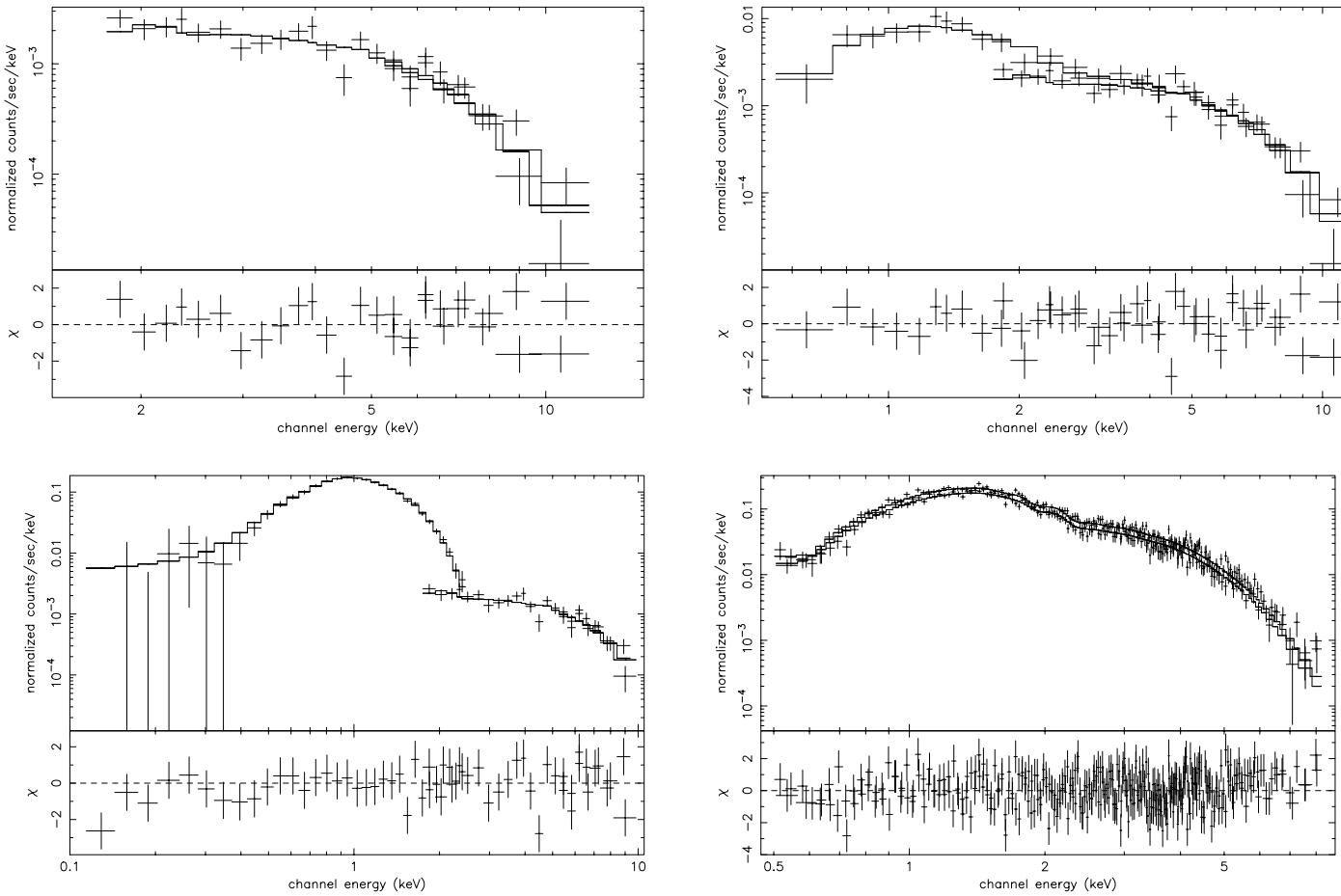

FIG. 7.—X-9 spectra, best-fit models and residuals in χ^2 units. *Upper left:* MECS (power law). *Upper right:* MECS + LECS (power law + MCBB). *Lower left:* PSPC + MECS (power law + MCBB). *Lower right: ASCA* (MCBB). Relevant parameters are in Table 4. *ASCA* data are from the two SIS detectors.

The spectral characteristics instead resemble those seen in some time-variable X-ray binaries (see e.g., Tanaka & Lewin 1995) and in particular are in very good agreement with those found for ultraluminous sources in spiral galaxies by Makishima et al. (2000).

Under this hypothesis we are observing a "low"-luminosity state with *SAX* and *ROSAT* ($L_{(0.5-2.4)} \sim 3 \times 10^{39}$) and a more luminous "high" state with *ASCA* ($L_{(0.5-2.4)} = 7.6 \times 10^{39}$ ergs s^{-1}). According to the model described by Esin, McClintock, & Narayan (1997), the high-state spectrum is dominated by a very hot disk, while in the low state the disk is either much colder or not visible at all. We have marginal evidence of its presence in the LECS + MECS spectrum, while the PSPC data clearly show a softer component that cannot be modeled with the simple power law used for the *SAX* data. As explained in § 3.3, we can reasonably assume that the spectrum does not change much between the PSPC and *SAX* observations and make a simultaneous fit of the two data sets. The best fit is then a power law plus an MCBB component, whose temperature is $\sim\frac{1}{3}$ of that found for *ASCA* data. This result suggests that some change in the structure of the emission region may have caused the observed change in the spectra.

The spectrum appears to be absorbed: the values of the $N_{\rm H}$ are compatible for all spectra (*ASCA*, *SAX*, and PSPC) and the mean value (weighted mean) is $0.18 \pm 0.02 \times 10^{22}$ cm^{-2}, that is $\sim$4 times the Galactic line of sight value. This excess could be due to the presence of a cold interstellar medium within the associated star-forming region (Miller & Hodge 1994).

4.1. *The "High State"*

The "high" state is crucial to derive some physical parameters of the system. In the hypothesis of an accreting black hole in the outer region of Holmberg IX, X-9 would be at a distance of 3.4 Mpc (from Georgiev 1991, the distance modulus of Holmberg IX is 27.67 and the extinction is negligible). In the *ASCA* data there is no evidence of a power-law continuum over the disk spectrum; this is consistent with the hypothesis that during the *ASCA* observation the disk was very close to the last stable orbit, and that its luminosity in the *ASCA* energy band was very high with respect to the reprocessed power-law continuum. We can then infer the inner radius directly from the normalization of the model as implemented in XSPEC. We find that, for a distance $D = 3.4$ Mpc, the inner radius is 183 ± 9 km, assuming a face-on geometry (otherwise this number scales as $(\cos\theta)^{-1/2}$, where θ is the inclination angle of the disk). For a Schwarzschild black hole the mass is related to the inner radius as

$$R_{\rm in} = \frac{6GM}{c^2} = 8.86\,\frac{M}{M_\odot}\ {\rm km}\ , \qquad (2)$$

which leads to a mass of $21 \pm 1\ M_\odot$. The bolometric luminosity can be evaluated from the relation between

maximum disk color temperature and inner radius, as in Makishima et al. (2000):

$$L_{\rm bol} = 4\pi(R_{\rm in}/\xi)^2\sigma(T_{\rm in}\kappa)^4 , \quad (3)$$

where σ is the Stefan-Boltzmann constant, $\kappa \sim 1.7$ is the ratio of the color temperature to the effective temperature ("spectral hardening factor"; e.g., Shimura & Takahara 1995), and $\xi = 0.412$ (Kubota et al. 1998) accounts for the fact that $T_{\rm in}$ occurs at a radius somewhat larger that $R_{\rm in}$. The above expression evaluated for the *ASCA* spectral parameters gives $L_{\rm bol} = 8.1 \times 10^{39}$; this is a factor of ~ 3 in excess of the Eddington luminosity limit for a $21 \pm 1\ M_\odot$ black hole that is

$$L_{\rm Edd} \sim \frac{4\pi G M m_p c}{\sigma_T} = 1.3 \times 10^{38}\ \frac{M}{M_\odot}$$
$$= 2.7 \pm 0.1 \times 10^{39}\ {\rm ergs\ s^{-1}}\ M_\odot^{-1} , \quad (4)$$

where M is the mass of the accretor, m_p is the mass of the proton, and σ_T is the Thomson cross section. Even assuming an accretion efficiency $\eta \sim 1$, we would need a black hole mass of at least $54\ M_\odot$ for the observed $L_{\rm bol}$ to be compatible with the Eddington limit (where $L_{\rm bol} = \eta L_{\rm Edd}$). We then find the same inconsistency, in the derived physical parameter of the source reported by Mizuno et al. (1999) for two ultraluminous sources in NGC 4565 and summarized by Makishima et al. (2000) for a larger sample of objects. Makishima et al. (2000) examine a number of possible solutions and suggest that if these objects are rapidly spinning black holes, the high temperature can be explained by the accretion disk getting closer to the black hole, and thus hotter.

As we do not have independent estimates of the distance of X-9, we discuss here the possibility that the distance is somehow overestimated. If X-9 is closer than 3.4 Mpc, we could explain the apparent inconsistency between the mass evaluated from the MCBB spectral parameters and that required assuming the Eddington limit. In fact these quantities scale as

$$M_{\rm Edd} \propto D^2 2\ {\rm cm}\ M_X \propto R_{\rm in} \propto D , \quad (5)$$

so that the ratio of these two mass estimates is proportional to the distance. In order to make the two mass estimates agree, we should have overestimated the distance of X-9 by a factor of at least 2.6 (assuming $\eta = 1$); this correction would give a distance of ~ 1.3 Mpc, and a new estimated accreting mass of $\sim 8\ M_\odot$, with a luminosity of $\sim 1.0 \times 10^{38}$ ergs s^{-1}. However, if we make this scenario even more realistic, we should take $\eta \sim 0.06$, which is the typical value assumed for Schwarzschild black hole efficiency. In this case we would get $D = 145$ kpc, $M = 0.88\ M_\odot$, i.e., not a black hole anymore, but a white dwarf. However, this results has severe drawbacks: the location of the source would be in the intergalactic space between the Milky Way and M81, a rather unusual location for an otherwise typical galactic source, and the spectrum we would expect from a source of this kind should be much softer than the one we actually observe, with a temperature of the order of 10^{-2} keV (see e.g., Kahabka 1998).

We can also exclude the possibility suggested by Stocke et al. (1994), from the study of MS 0317.7−6647, located in the vicinity of NGC 1313. The authors suggest that this source could be inside our Galaxy, at the distance of ~ 150 pc, being an old isolated neutron star that is no longer rotating or pulsing, but is still emitting X-rays by slow accretion of interstellar gas onto its magnetic poles from the thick surrounding interstellar matter. If this were the case of X-9 too, the luminosity would be of the order of 10^{31} ergs s^{-1}. However, if the spectrum observed with *ROSAT* is in the temperature range predicted for this kind of sources (Colpi, Campana, & Treves 1993), the *ASCA* spectrum is much too hard. Moreover, the presence of the power law detected with *SAX*/MECS cannot be justified by this model, and the same holds for the spectral variability we observe between *SAX* and *ASCA* observations.

If we retain the location of the source to be in Holmberg IX (i.e., at a distance of 3.4 Mpc), we can follow the argumentation put forward by Makishima et al. (2000), who make the hypothesis that the accreting object is a Kerr black hole. In this case the disk can come closer to the central mass, and the last stable orbit can go down to 0.5 Schwarzschild radii, implying that the temperature can get higher, even if we neglect any strong relativistic effects. To apply this simple correction to our results, we remind that the last stable orbit radius of a rotating black hole is related to the mass as

$$R_{\rm in} = \alpha\ \frac{6GM}{c^2} = 8.86\alpha\ \frac{M}{M_\odot}\ {\rm km} \quad (6)$$

where $\frac{1}{6} < \alpha < 1$. In the extreme case of $\alpha = \frac{1}{6}$, corresponding to a maximally rotating black hole, we get $M = 126\ M_\odot$. This mass implies $L_{\rm Edd} = 1.9 \times 10^{40}$ ergs s^{-1}, which agrees well with the measured bolometric luminosity $L_{\rm bol}$ if we assume a radiation efficiency of $\eta \sim 0.4$ ($L_{\rm bol} = \eta L_{\rm Edd}$), as can be reached by a maximally rotating Kerr black hole fed with a prograde disk (see, e.g., Shakura & Sunyaev 1973).

Therefore, while the model of a nonrotating black hole leads to severe drawbacks, the hypothesis of a rotating Kerr black hole, along the line suggested by Makishima et al. (2000), may give a more self-consistent scenario, leading to a $126\ M_\odot$ black hole. It is worth noting that the existence of black holes of this mass is still quite controversial, being much smaller than galactic nuclear black holes (10^7–$10^8\ M_\odot$) and much larger than stellar sizes black holes ($10\ M_\odot$), thus suggesting new interesting scenarios to massive black holes formation. Madau & Rees (2001) suggested that such objects, with masses $\gtrsim 150\ M_\odot$ can be the end product of pregalactic star formation episodes: their progenitors would be zero-metallicity (Population III) very massive stars. The high-mass limit would be relaxed to smaller values if X-9 is a beamed source. Beaming in ultraluminous galactic sources has recently been advanced as an alternative scenario to the very massive black hole hypothesis (King et al. 2001)

4.2. *The "Low" State*

The nearly constant PSPC hardness ratios and the good agreement between PSPC and LECS spectra suggest that no significant spectral changes have occurred in the soft X-ray emission from X-9 during the "low state" observations.

The PSPC and *SAX*(MECS+LECS) spectra can be well described with a MCBB model with temperature $T \sim 0.28$ keV plus a power law with photon index $\Gamma \sim 1.35$.

The spectral features resemble those observed in the low state of galactic black hole candidate, such as the well-studied Cyg X-1 (see, e.g., Gierlinski et al. 1999; Frontera et

al. 2001), Nova Muscae (Esin et al. 1997), or Sgr A* (Narayan, Yi, & Mahadevan 1996). These sources are observed to spend most of their time in a low-intensity state, characterized by a power-law continuum and, for high enough accretion rates, a soft thermal component arising from the accretion disk. In most cases there is also evidence of fluorescent emission from Fe, with the detection of a line at 6.4 keV. These features are interpreted in the framework of the ADAF (advection-dominated accretion flow; see, e.g., Esin et al. 1997) model as the signature of a geometry where the disk is truncated far from the last stable orbit, and in the region between the disk and the compact object (the ADAF region) a substantial part of the energy is stored in the accreting gas rather than being radiated. When the accretion rate grows over a critical value, the ADAF disappears and the disk approaches the last stable orbit. In this high state the emission is dominated by the disk thermal spectrum, in a way similar to what we observe in the *ASCA* spectrum of this source.

However, the power-law index predicted by the ADAF model (and observed in the sources above – $\Gamma \gtrsim 1.5$) for the low state is larger than the index we measure in our data, suggesting that this model may not be entirely adequate to describe our source. A behavior closer to that of X-9 was observed with *ASCA* in 1E 1740.7−2942, a bright source near to the Galactic center (Sakano et al. 1999; Sidoli et al. 1999). The broadband spectrum of this source strongly suggests that it is indeed a stellar mass black hole. Sakano et al. (1999) find that the 2.0–10.0 keV spectrum can be described with a power law of photon index Γ in the range 0.9–1.3. They do not find any evidence of thermal component, but this could be due to the harder energy band they use in their analysis (2.0–10.0 keV vs. 0.2–10.0 keV of our data). This source, indeed, shows no evidence for a line at 6.4 keV. Interestingly, similarly flat power-law spectra are found in the super-Eddington sources discovered with Chandra in the Antennae galaxies (Fabbiano, Zezas, & Murray 2001; Zezas et al. 2001, in preparation).

In summary, the low-state spectrum of X-9 resembles closely the spectra of other black hole candidates in their low state, with the only difference of a slightly flatter power-law index.

5. CONCLUSIONS

We have analyzed all the available X-ray observations of the M81 region in order to understand the nature of the ultraluminous X-ray source M81 X-9. Our results can be summarized as follows:

1. The X-ray source is a pointlike object, possibly surrounded by a faint diffuse medium, that could account for about 10% of the total emission. This result needs a more accurate verification, that can only come from observations with high-resolution X-ray cameras, like those onboard the *Chandra Observatory*. The optical counterpart appears to be a faint blue object embedded in a Hα cloud. The nature of this object is still unclear, and optical observations are also needed to clarify this point.
2. The flux of X-9 is strongly variable and this variability points to a compact object. This source was observed over 20 yr with *Einstein*, *ROSAT*, *ASCA* and *BeppoSAX*, with almost continuous coverage during the last 8 yr. The light curves show nonperiodic flux variations of up to a factor of 4.
3. The *ROSAT*/PSPC and *SAX* data were all collected during low-intensity states ($L_X \sim 4 \times 10^{39}$ ergs s^{-1}) and have consistent spectral distributions, while the high-state *ASCA* spectrum ($L_X \sim 8 \times 10^{39}$ ergs s^{-1}) is significantly different. The observed spectrum can be well fitted with a MCBB model with $T \sim 1.24$ keV for the high-state *ASCA* data and with a colder ($T \sim 0.3$keV) MCBB plus a flat ($\Gamma \sim 1.3$) power law for the PSPC and *SAX* data.
4. The intensity and spectral variability of X-9 supports the scenario of an accreting black hole binary. From the *ASCA* best-fit parameters we infer a Kerr black hole mass of $\sim 126\ M_\odot$, if at the distance of 3.4 Mpc and assuming nonbeamed X-ray emission.

We thank Andreas Zezas for discussions on ultraluminous sources in galaxies, Sam Dyson for help in the initial *ROSAT* data reduction, and Rosario Iaria for discussions on accretion processes. This work was supported in part by NASA grant NAG 5-2946 and NASA contract NAS 8-39073(CXC) and in part by MURST. This research has made use of the HEASARC online database and of the ESO online DSS.

REFERENCES

Arnaud, K. A., George, I. M., & Tennant, A. F. 1992, Legacy, 2, 65
Beck, R., Klein, U., & Krause, M. 1985, A&A, 152, 237
Bietenholz, M. F., et al. 1996, ApJ, 457, 604
Boella, G., Butler, R. C., Perola, G. C., Piro, L., Scarsi, L., Bleeker, J. A. M. 1997, A&AS, 122, 299
Boese, F. G. 2000, A&AS, 141, 507
Burke, B. E., et al. 1991, IEEE Trans. ED-38, 1069
Collura, A., Maggio, A., Sciortino, S., Serio, S., Vaiana, G. S., & Rosner, R. 1987, ApJ, 315, 340
Colpi, M., Campana, S., & Treves A. 1993, A&A, 278, 690
Damiani, F., Maggio, A., Micela, G., & Sciortino, S 1997, ApJ, 483, 370
David, L.P., et al. 1996, in The *ROSAT* Users Handbook, ed. U. G. Briel et al. (Garching: MPE)
Esin, A. A., McClintock, J. E, & Narayan R. 1997, ApJ, 489, 865
Ezoe, Y., Iyomoto, N., & Makishima K. 2000, PASJ, 53, 69
Fabbiano, G. 1988, ApJ, 325, 544
———. 1995, in X-Ray Binaries, ed. Lewin, van Paradjis, van der Heuvel (Cambridge: Cambridge Univ. Press), 390
Fabbiano, G., Zezas, A., & Murray, S. S. 2001, ApJ, in press
Freedman, W. L., et al. 1994, ApJ, 427, 628
Frontera, F., et al. 2001, ApJ, 546, 1027
Georgiev, Ts. B., Bilkina, B. I., Tikhonov, N. A., & Karachentsev, I. 1991, A&AS, 89, 529
Giacconi R., et al. 1979, ApJ, 230, 540
Gierlinski, M. Zdziarski, A. A., Poutanen, J., Coppi, P. S., Ebisawa, K., & Johnson, W. N. 1999, MNRAS, 309, 496
Harris, D. E., Silverman, J. D., Hasinger, G., & Lehman, I. 1998, A&AS, 133, 431
Henkel, C., Stickel, M., Salzer, J. J., Hopp, U., Brouillet, N., & Baudry, A. 1996, A&A, 273, L15
Hill, J. K., et al. 1993, ApJ, 402, L45
Ho, L. C., Filippenko, A. V., & Sargent, W. L. W. 1996, ApJ, 462, 183
Ishisaki, Y., et al. 1996, PASJ, 48, 237
Kahabka, P., 1998, A&A, 332, 189
King, A. R., Davies, M. B., Ward, M. J., Fabbians, G., & Elvis, M. 2001, ApJ, 552, L109
Kohmura, Y., et al. 1993, Proc. SPIE, 2006, 79
Kubota A., Tanaka, Y., Makishima, K., Ueda, Y., Dotani, T., Inoue, H., & Yamaoka, K. 1998, PASJ, 50, 667
Madau, P., & Rees, M. J. 2001, ApJ, 551, L27

Mackie, G., et al. 1995, in ASP Conf. Ser. 77, Astronomical Data Analysis Software and Systems IV, ed. R. A. Shaw, H. E. Payne, & J. J. E. Hayes (San Francisco: ASP)
Makishima, K., et al. 2000, ApJ, 535, 632
Miller, B. W. 1995, ApJ, 446, L75
Miller, B. W., & Hodge, P. 1994, ApJ, 427, 656
Mizuno, T., Ohnishi, T., Kubota, A., Makishima, K., & Tashiro, M. 1999, PASJ, 51, 663
Narayan, R., Yi, I., & Mahadevan, R. 1996, A&AS, 120, 287
Parmar, A. N., et al. 1997, A&AS, 122, 309
Pellegrini, S., Cappi, M., Bassani, L., Malaguti, G., Palumbo, G. G. C., & Persic, M. 2000, A&A, 353, 447
Pfeffermann, E., et al. 1987, Proc. SPIE, 733 (519), 117
Piro, L., Matt, G., & Ricci, R. 1997, A&AS, 126, 525
Reynolds, C. S., 1997, MNRAS, 286, 513
Sakano, M., Imanishi, K., Tsujimoto, M., Koyama, K., & Maeda, Y. 1999, ApJ, 520, 316
Shakura, N.I., & Sunyaev, R.A. 1973, A&A, 24, 337
Shimura, T., & Takahara, F. 1995, ApJ, 445, 780
Sidoli, L., Mereghetti, S., Israel, G. L., Chiappetti, L., Treves, A., & Orlandini, M. 1999, ApJ, 525, 215
Snowden, S. L. McCammon, D., Burrows, D. N., & Mendenhall, J. A. 1994, ApJ, 424, 714
Stocke, J. T., Wang, Q. D., Perlman, E. S., Donahue, M., & Schachter, J. 1994, in The Soft X-Ray Cosmos, Proc. *ROSAT* Science Symp., ed. E. Schlegel & R. Petre (New York: AIP), 7
Tanaka, Y., Inoue, H., & Holt, S .S. 1994, PASJ, 46, L37
Tanaka, Y., & Lewin, W. H. G. 1995, in X-Ray Binaries, ed. Lewin, W. H. G. van Paradjis, J., & van der Heuvel, E. (Cambridge: Cambridge Univ. Press), 390
Tody, D. 1986, Proc. SPIE 627, 733
Wang, D., & Chu, Y. 1999, AAS, 194, 64.09
Wang, Q., & Helfand, D. J. 1991, ApJ, 379, 327
Worral, D. M., et al. 1992, in Data Analysis in Astronomy IV, ed. V. di Gesù New York: Plenum)